



Universiteit
Leiden
The Netherlands

Novel pathways in cholesterol metabolism to combat cardiometabolic diseases

Zhou, E.

Citation

Zhou, E. (2021, April 28). *Novel pathways in cholesterol metabolism to combat cardiometabolic diseases*. Retrieved from <https://hdl.handle.net/1887/3161375>

Version: Publisher's Version

License: [Licence agreement concerning inclusion of doctoral thesis in the Institutional Repository of the University of Leiden](#)

Downloaded from: <https://hdl.handle.net/1887/3161375>

Note: To cite this publication please use the final published version (if applicable).

Cover Page



Universiteit Leiden



The handle <http://hdl.handle.net/1887/3161375> holds various files of this Leiden University dissertation.

Author: Zhou, E.

Title: Novel pathways in cholesterol metabolism to combat cardiometabolic diseases

Issue date: 2021-04-28



**Inhibition of DHCR24 ameliorates hepatic steatosis and inflammation
through LXR α without inducing hyperlipidemia**

Enchen Zhou, Hiroyuki Nakashima, Rumei Li, Hendrik J.P. van der Zande,
Cong Liu, Zhuang Li, Christoph Müller, Franz Bracher,
Yassene Mohammed, Jan Freark de Boer, Folkert Kuipers, Bruno Guigas,
Patrick C.N. Rensen, Martin Giera, Yanan Wang

Submitted

Abstract

Background

Liver X receptor (LXR) agonism has theoretical potential for treating NAFLD/NASH but synthetic agonists induce lipogenesis and hyperlipidemia in preclinical models. Desmosterol, which is converted by $\Delta 24$ -dehydrocholesterol reductase (DHCR24) into cholesterol, is a potent endogenous LXR agonist with anti-inflammatory properties. We aimed to investigate the effects of selective DHCR24 inhibition by SH42 on hepatic steatosis and inflammation, two main hallmarks of NAFLD/NASH, in relation to lipidemia.

Methods and results

Male *APOE*3-Leiden.CETP* mice, a well-established translational model for lipoprotein metabolism that develops diet-induced human-like NAFLD/NASH characteristics, were fed a high fat and high cholesterol diet with or without simultaneous treatment with SH42, a selective DHCR24 inhibitor. After 8 weeks, SH42 treatment markedly increased liver and plasma desmosterol levels without influencing food intake, body weight or body composition. SH42 markedly reduced the steatosis score (-58%), hepatic diacylglycerol (DAG) (-20%) and triacylglycerol (TAG) (-39%) contents as well as the number of crown-like structures (-79%) in the liver. Flow cytometry analysis showed that SH42 decreased liver inflammation by preventing Kupffer cell activation (-71%) and monocyte infiltration (-79%). Interestingly, SH42 reduced plasma free fatty acid (-16%) and cholesteryl ester (-24%) concentrations without concomitant changes in DAG and TAG levels. *LXR* α -deficiency completely abolished the beneficial effects of SH42 on liver lipid levels, steatosis score and liver inflammation.

Conclusions

Inhibition of DHCR24 by SH42 leads to an increase in desmosterol and prevents diet-induced hepatic steatosis and inflammation in a strictly *LXR* α -dependent manner without causing hyperlipidemia. We anticipate that pharmacological DHCR24 inhibition may represent a potential novel therapeutic strategy for treatment of NAFLD/NASH.

Introduction

Non-alcoholic fatty liver disease (NAFLD) comprises a spectrum of diseases ranging from simple hepatic steatosis to non-alcoholic steatohepatitis (NASH). The latter is characterized by steatosis, hepatocellular damage and inflammatory cell infiltration with or without fibrosis. Hepatic steatosis is defined as accumulation of primarily neutral lipids such as triacylglycerols (TAG) and cholesteryl esters (CE) in the form of lipid droplets within hepatocytes as well as non-parenchymal liver cells, including Kupffer cells (KCs) [1]. Hepatic steatosis results from an imbalance between lipid uptake, synthesis, secretion and lipolysis, and is usually associated with dyslipidemia, insulin resistance, hypertension, type 2 diabetes and obesity [2]. The essential trigger for the transition of simple steatosis to NASH is not yet completely elucidated. Despite the high global prevalence of NAFLD (25.2%) in the general population [3], no FDA-approved medication is available yet for the treatment of NAFLD/NASH. In fact, lifestyle adjustment is still the main clinical intervention.

Inflammation contributes to the transition of simple steatosis to NASH and liver-resident KCs play a pivotal role in NAFLD/NASH pathogenesis [4]. Once activated during NAFLD progression, KCs produce pro-inflammatory factors, such as monocyte chemoattractant protein 1 (MCP-1) and tumor necrosis factor (TNF), leading to increased hepatic monocyte recruitment and inhibition of canonical insulin signaling, further aggravating liver injury and steatosis [5, 6]. In addition, KC-derived pro-fibrinogenic factors increase collagen production by hepatic stellate cells, generating a vicious circle that exacerbates NAFLD and inflammation, and derive progression towards NASH [7, 8]. Thereby, selective depletion of KCs from the liver alleviates hepatocellular damage and prevents diet-induced hepatic steatosis and insulin resistance [9, 10]. Furthermore, consumption of a cholesterol-rich diet causes cholesterol accumulation in KCs to yield foamy inflammatory KCs, which directly contribute to liver inflammation [11]. More recently, NAFLD/NASH was shown to impair KC self-renewal and induce KC death, thus reducing embryonically-derived liver-resident KCs [12, 13]. This KC niche is replenished through recruitment, differentiation, and proliferation of monocyte-derived macrophages, which are however reported to be more inflammatory than KCs and to contribute to aggravation of liver inflammation and damage [12, 13].

Liver X receptors (LXRs), *i.e.*, the LXR α and LXR β isoform, are essential (oxy)sterol-activated transcription factors involved in lipid metabolism and immune responses [14, 15]. LXR α is abundantly expressed in liver, adipose tissue, and macrophages, while LXR β is ubiquitously expressed [16]. In macrophages, LXR α directly promotes reverse cholesterol transport via up-regulating ATP binding cassette (ABC) A1 [17]. Thus, LXR α -deficiency impairs cholesterol efflux and is associated with increased atherosclerosis [18, 19]. Simultaneously, LXRs exert anti-inflammatory effects in immune cells [20], suppress KC activation, and protect against hepatic injury [21]. In addition, LXRs promote formation of long chain polyunsaturated fatty acids (PUFAs), *e.g.* eicosapentaenoic acid and docosahexaenoic acid, which have anti-inflammatory activities [22, 23]. The simultaneous regulation of lipid metabolism and inflammation serves LXRs as a potential drug targets for NAFLD/NASH treatment [14, 15]. However, at present no selective LXR agonists exist for the clinical treatment of NAFLD/NASH. This is mainly due to unfavorable effects of pharmacological LXR activation on sterol regulatory element-binding proteins (SREBPs)-induced lipogenesis, resulting in elevated atherogenic low density lipoprotein (LDL) cholesterol and triglycerides. Therefore, rather than alleviating liver lipid levels, most synthetic LXR agonists actually cause hepatic steatosis and hypertriglyceridemia [24, 25]. Moreover, some synthetic LXR agonists have been reported to cause neutropenia due to down-regulation of neutrophil production in bone marrow and stimulation of their clearance by macrophages within peripheral tissues [26]. Taken together, a

successful drug candidate for the treatment of NASH through LXR activation, should be LXR selective, not induce *sterol regulatory element-binding transcription factor 1* (*Srebf1*), and not cause neutropenia.

Previously, we reported that synthetic SH42 inhibits $\Delta 24$ -dehydrocholesterol reductase (DHCR24), an important enzyme intertwining the Bloch and Kandutsch-Russell pathways of distal cholesterol biosynthesis, and causes accumulation of desmosterol [27]. Importantly, both in steady-state macrophages and foam cells, desmosterol increases LXR target genes while inhibiting SREBP target genes [28, 29]. Accordingly, we have recently reported that selective inhibition of DHCR24 induces LXR activation through accumulation of desmosterol, promoting resolution of inflammation without affecting *Srebf1c* expression in macrophages [23, 30]. Taken together, we hypothesized that inhibiting DHCR24 leads to increased desmosterol levels and subsequently induces LXR activation in KCs, thereby suppressing inflammation, without inducing lipid synthesis via *Srebf1*. Using our novel and selective DHCR24 inhibitor SH42 [30], we aimed to investigate the potential therapeutic effects of DHCR24 inhibition on diet-induced NAFLD development in APOE*3-Leiden.CETP mice, a well-established humanized mouse model for study of (cardio)metabolic diseases.

Materials and methods

Animals and treatments

Hemizygous *APOE*3-Leiden* (*E3L*) mice were crossbred with homozygous human cholesteryl ester transfer protein (CETP) transgenic mice to generate heterozygous *E3L.CETP* mice on a C57BL/6J background [31]. LXR α -deficient mice (also on C57BL/6J background), generated by Deltagen using gene-targeting methods as described [32], were kindly provided by Tularik (San Francisco, CA, US). Mice were group-housed in individually ventilated cages in standard conditions at room temperature (22°C) with 40 \pm 5% relative humidity and a 12-h light/dark (7 am lights on; 7 pm lights off) cycle. Water and standard laboratory diet (801203, Special Diets Services, UK) were available *ad libitum*, unless indicated otherwise. This study was approved by the Animal Ethical Committee of Leiden University Medical Center, Leiden, The Netherlands (AVD1160020173305, PE.18.034.007) and the Animal Ethical Committee of University Groningen, Groningen, The Netherlands (PE.18.034.030, 173305-02-001). All animals received humane care according to the criteria outlined in the NIH “Guide for the Care and Use of Laboratory Animals”. All animal procedures were performed conform the guidelines from Directive 2010/63/EU of the European Parliament on the protection of animals used for scientific purposes.

At the age of 10-12 weeks, male *E3L.CETP* mice and LXR α -deficient mice were fed a high fat high cholesterol diet (HFCD; Altromin, Germany) containing 60% (energy) fat and 1% (wt/wt) cholesterol, and were randomized into two groups treated with either the DHCR24 inhibitor SH42 (0.5 mg·mouse⁻¹) [23, 30] or vehicle (saline containing 3.3% ethanol and 3.3% Cremophor EL) 3 times per week by intraperitoneal injection. *E3L.CETP* mice were treated for 4 weeks (n= 6 mice per group) and 8 weeks (n= 8 mice per group) to evaluate effects on hepatic immune cells via flow cytometry analysis and hepatic steatosis via quantitative lipidomic analysis, respectively. LXR α -deficient mice were treated with either SH42 (n= 11 mice) or vehicle (n= 10 mice) for 4 weeks to evaluate effects on hepatic steatosis and immune cells.

Body weight was measured weekly. Body composition (*i.e.* fat body and lean body mass; EchoMRI-100; EchoMRI, Houston, TX, USA) was evaluated before and after intervention.

Food intake was determined during the treatment period.

Details of all parameters measured in each study are provided in the **Supplemental appendix**.

Statistical analysis

For the volcano plots, Wilcoxon rank sum test (Mann Whitney Wilcoxon Test) was used to compare concentrations of lipid species, and fold change was calculated based on median values in each group. Due to the excellent precision of the applied analytical approach (Lipidizer™) [33], the log₂ fold change threshold was put to 0.5 corresponding to a change of 1.4 in median concentration between the groups. This change is reproducibly measurable using the sample analysis method we applied here [33]. p-value threshold was put to 0.05 corresponding to 1.301 on the volcano plot y-axis. For the Wilcoxon rank sum test and fold change calculations the control group was used as reference. Lipid classes were used in the volcano plots for the assignment of colours. Outliers were identified using Grubbs' test (<https://www.graphpad.com/quickcalcs/Grubbs1.cfm>) and removed from statistical analysis, which is clearly stated in figure legends if applicable. Differences between two groups were compared using Student's t-tests performed in GraphPad Prism 8.1 (GraphPad Software). $p < 0.05$ was considered significant (* $p < 0.05$, ** $p < 0.01$, *** $p < 0.001$).

Results

Inhibition of DHCR24 by SH42 markedly increases liver desmosterol levels and ameliorates hepatic steatosis

To assess the effects of DHCR24 inhibition on hepatic steatosis, *E3L.CETP* mice were fed a HFCD while being treated with vehicle or the synthetic DCHR24 inhibitor SH42 [23, 30] for a period of 8 weeks. SH42 treatment did not affect food intake (**Supplemental Figure 1A**), while temporarily preventing HFCD-induced body weight gain as compared to control group (**Supplemental Figure 1B**). After 8 weeks of treatment, body weight and body composition, *i.e.*, lean body mass (**Supplemental Figure 1C**) and fat body mass (**Supplemental Figure 1D**) of SH42 treated mice was comparable to that of the control group. In addition, the weight of various tissues (*i.e.*, liver, white adipose tissue, kidney, heart, lung, spleen, and brown adipose tissue) was unchanged by SH42 treatment (**Supplemental Figure 1E**). As anticipated, SH42 markedly increased hepatic desmosterol levels (10-fold, **Figure 1A**, **Supplemental Figure 1F**).

Hepatic steatosis was evaluated by HE staining and scored as detailed previously [34]. As compared to the control treatment, SH42 treatment ameliorated diet-induced hepatic steatosis (**Figure 1B**), as evident by a clear reduction of the hepatic steatosis score (-58%, **Figure 1C**), and liver lipid area (-35%, **Figure 1D**). We next analysed liver lipid profiles by comprehensive lipidomic analysis. Firstly, we observed a clear alteration in the lipid class composition after SH42 treatment (**Figure 1E**). Specifically, SH42 treatment caused a relative reduction of TAG (-21%) and DAG (-22%), accompanied by a relative increase of the other lipid classes, including CER, PC, PE, and SM (**Figure 1E**, **Supplemental Figure 2**). Volcano plot analysis of the lipid species concentrations of different lipidomes revealed the effects of SH42 treatment on the individual hepatic lipid species. The majority of significantly altered lipid species were down-regulated, and most of them were TAGs (**Figure 1F**). Consistently, SH42 decreased hepatic concentrations of TAG (-39%, **Figure 1G**) and DAG (-20%, **Figure 1H**). In addition, SH42 treatment tended to reduce hepatic FFA (-16%; $p = 0.07$, **Figure 1I**) and CE levels (-25%; $p = 0.07$, **Figure 1J**). Despite these strong effects on hepatic lipid content, SH42

did not affect fasting plasma glucose, insulin, or homeostatic Model Assessment for Insulin Resistance (HOMA-IR) scores (**Supplemental Figure 1G-I**). Taken together, inhibition of DHCR24 by SH42 markedly increases liver desmosterol levels, accompanied by amelioration of diet-induced hepatic steatosis without marked effects on body composition and glucose homeostasis.

Inhibition of DHCR24 by SH42 prevents Kupffer cell activation and reduces immune cell infiltration into the liver

We next evaluated the effect of DHCR24 inhibition on the hepatic inflammation in mice treated with SH42 or vehicle for 8 weeks by immunohistochemistry. SH42 treatment significantly reduced the hepatic F4/80 content (-29%, **Figure 2A, B**) as well as the number of hepatic crown-like structures of macrophages surrounding dying hepatocytes (-79%, **Figure 2C**), which is a prominent feature of NASH development [35].

Flow cytometry on MACS-purified hepatic leukocytes revealed that 4 weeks SH42 treatment tended to decrease total hepatic leukocytes (-37%; $p=0.09$, **Figure 2D**). Given the critical role of KCs in the progression of NASH [9, 10], we next explored the effects of DHCR24 inhibition on KCs. We observed a tendency towards increased total KCs upon SH42 treatment (+44%; $p=0.06$, **Figure 2E, F**). Strikingly, SH42 relatively reduced MHCII⁺/CD11c⁺ activated KCs (-71%; **Figure 3G, H**) accompanied by an increase in MHCII⁺/CD11c⁻ resting KCs (+21%, **Figure 3G, I**), indicative of prevented KC activation. In addition, SH42 treatment reduced monocytes in both liver (-79%, **Figure 2J**) and blood (-43%; $p=0.08$, **Supplemental Figure 3A, B**), and induced a trend for decreased hepatic neutrophils (-50%; $p=0.06$, **Figure 2K**) without affecting circulating neutrophils (**Supplemental Figure 3A, C**). Together, these data indicate that SH42 treatment prevents KC activation, limits hepatic immune cell recruitment and dampens hepatic inflammation.

Inhibition of DHCR24 by SH42 does not increase circulating lipids

Consistent with the potent increase in hepatic desmosterol levels, SH42 also markedly increased plasma desmosterol levels from undetectable levels ($< 0.5 \mu\text{g}\cdot\text{mL}^{-1}$) to $3.1 \pm 0.4 \mu\text{g}\cdot\text{mL}^{-1}$ (**Figure 3A**). Since synthetic LXR agonists usually induce lipogenesis and hypertriglyceridemia as unwanted effects [24, 26], we next determined the effect of 8 weeks of SH42 treatment on circulating lipid levels using quantitative comprehensive lipidomic analysis. Analysis of the plasma lipidome revealed that SH42 treatment relatively decreased circulating CE while relatively increasing LCER, PC and PE (**Supplemental Figure 4**). With respect to absolute lipid concentrations, SH42 did not affect plasma levels of total TAG (**Figure 3B**) and DAG (**Figure 3C**), while significantly decreasing plasma levels of FFA (-16%, **Figure 3D**) and CE (-24%, **Figure 3E**). These data imply that inhibition of DHCR24 by SH42 increases plasma desmosterol levels and decreases FFA and CE levels, importantly without inducing hypertriglyceridemia.

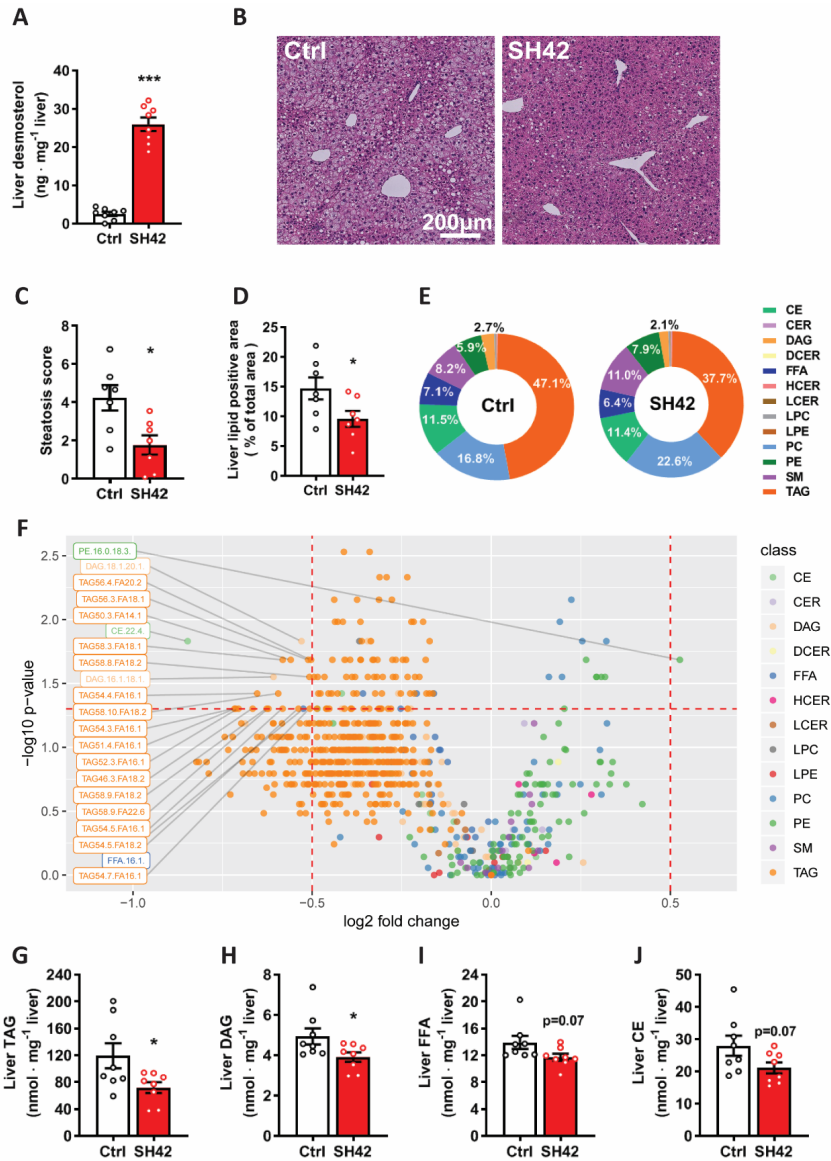


Figure 1. Inhibition of DHCR24 by SH42 markedly increases liver desmosterol and ameliorates hepatic steatosis. *E3L.CETP* mice fed a high fat high cholesterol diet (HFCD) were treated with vehicle or DHCR24 inhibitor SH42 (n= 8 mice per group). After 8 weeks of treatment, mice were sacrificed and livers were collected (**A**) to measure desmosterol levels, and (**B**) to stain with haematoxylin and eosin (HE). (**C**) Hepatic steatosis was scored and (**D**) lipid positive area was quantified (n= 7 mice per group; two values were identified as outliers based on Grubbs' test and removed from statistical analysis). (**E**) Liver lipid classes were analysed (Supplemental Figure 2), and the relative average abundance of lipid classes in each group are depicted as pie charts. (**F**) Volcano plot analysis of liver lipid species concentrations is shown. Annotated lipid species are characterized by a fold change >1.4 or <0.7 (SH42/Ctrl) and a p value <0.05. Hepatic (**G**) TAG, (**H**) DAG, (**I**) FFA and (**J**) CE lipid class concentrations were summarized. Values are mean \pm SEM. Differences between two groups were determined

using unpaired Student's t-test if not indicated otherwise. * $p < 0.05$, *** $p < 0.001$ vs. control (ctrl). Abbreviations: CE, cholesteryl esters; CER, ceramides; DAG, diacylglycerols; DCER, dihydroceramides; FFA, free fatty acids; HCER, hexosylceramides; LPC, lysophosphatidylcholines; LPE, lysophosphatidylethanolamines; PC, phosphatidylcholines; PE, phosphatidylethanolamines; SM, sphingomyelins; TAG, triacylglycerols.

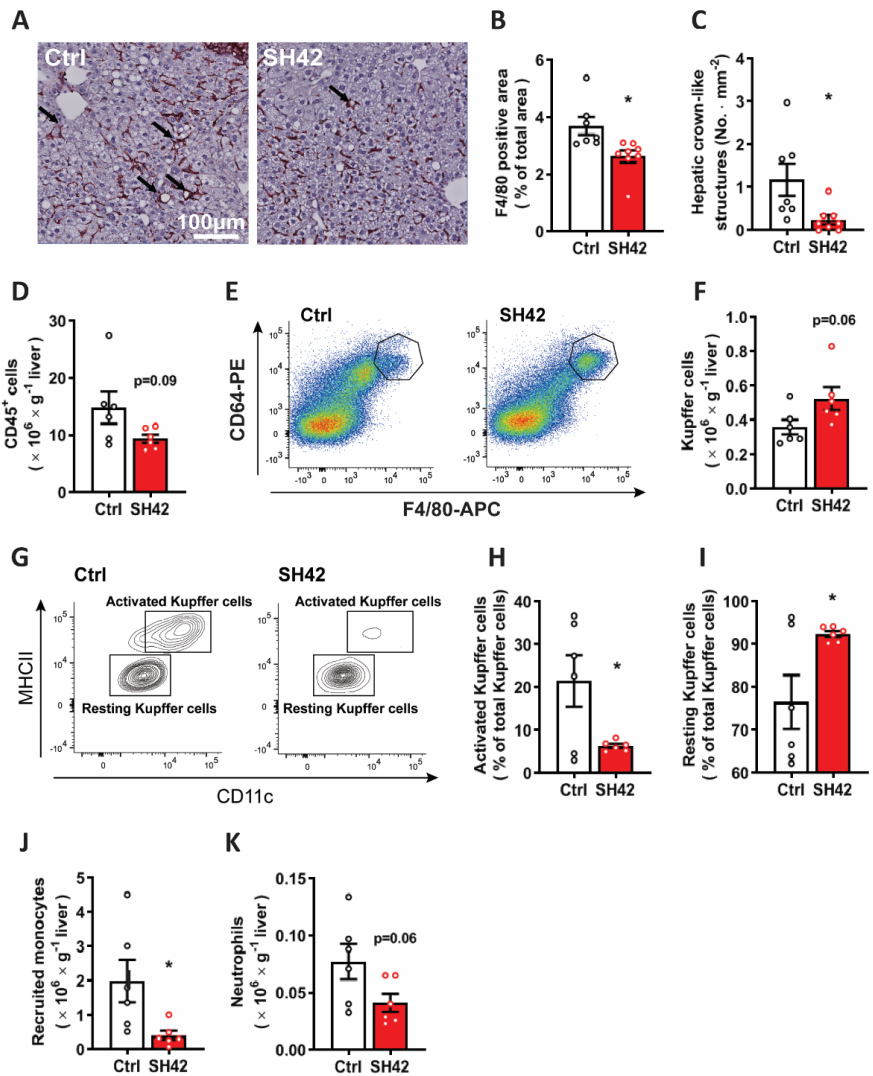


Figure 2. Inhibition of DHCR24 by SH42 prevents Kupffer cell activation and reduces immune cell infiltration into the liver. *E3L.CETP* mice fed a HFD were treated with vehicle or DHCR24 inhibitor SH42 (n= 8 mice per group). After 8 weeks of treatment, mice were sacrificed and livers were collected to stain with F4/80. (A) Representative pictures of F4/80 staining are shown and (B) F4/80 positive area was quantified. (C) Hepatic crown-like structures were counted (n= 7 and 8 mice, respectively; one value was identified as an outlier based on a Grubbs' test and removed from statistical analysis). In another experiment after 4 weeks of treatment (n= 6 mice per group), fresh livers were collected to isolate and count

(D) CD45⁺ cells. (E and F) Total Kupffer cells (KCs), (G and H) activated KCs, (G and I) resting KCs, (J) recruited monocytes, and (K) neutrophils in the liver were measured via flow cytometry. Values are mean \pm SEM. Differences between two groups were determined using unpaired Student's t-test. * p <0.05 vs. ctrl.

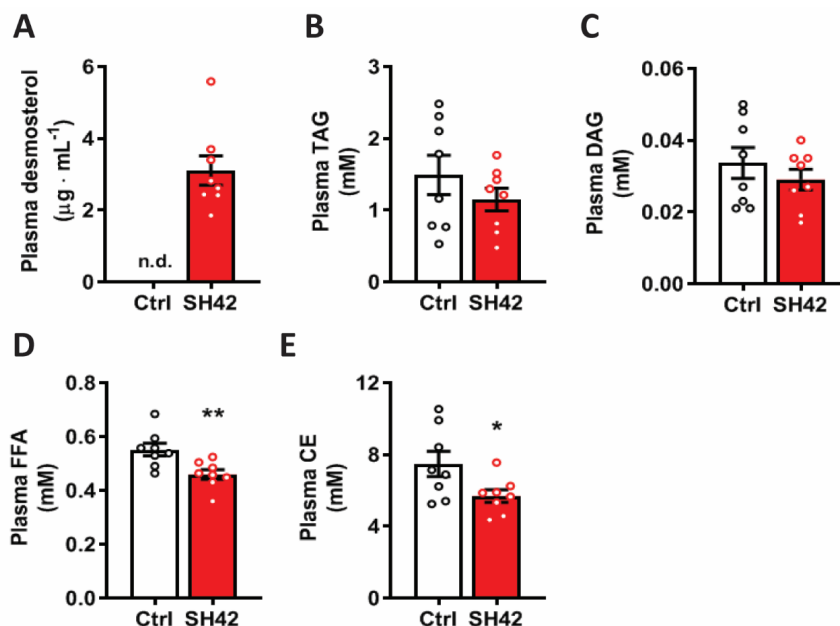


Figure 3. Inhibition of DHCR24 by SH42 does not increase circulating lipids. *E3L.CETP* mice fed a HFD were treated with vehicle or DHCR24 inhibitor SH42 ($n=8$ mice per group). After 8 weeks of treatment, blood was collected to measure (A) desmosterol levels and for quantitative lipidomic analysis. Plasma (B) TAG, (C) DAG, (D) FFA and (E) CE lipid class concentrations were summarized. Values are mean \pm SEM. Differences between two groups were determined using unpaired Student's t-test. * p <0.05, ** p <0.01 vs. ctrl. Abbreviations: CE, cholesteryl ester; DAG, diacylglycerols; FFA, free fatty acids; TAG, triacylglycerols.

The therapeutic effects of DHCR24 inhibition on hepatic steatosis are strictly dependent on LXR α

Based on previous reports [23, 28, 29], we hypothesized that the therapeutic effects of SH42 were attributed to LXR activation triggered by increased desmosterol levels as a result of DHCR24 inhibition. Since LXR α plays a crucial role in both lipid metabolism [36] and macrophage/KC homeostasis [18, 19, 37], we next evaluated the effects of 4 weeks of SH42 treatment in HFCD-fed LXR α -deficient mice to evaluate the importance of LXR α in the observed protective effects of SH42 in ameliorating hepatic steatosis and inflammation. SH42 treatment had no effect on body weight (**Supplemental Figure 5A**), body composition (**Supplemental Figure 5B, C**) or liver weight (**Supplemental Figure 5D**) in LXR α -deficient mice. Consistent with previous findings that LXR α -deficient mice are more susceptible to high fat diet-induced hepatic steatosis and inflammation [37, 38], we observed significant hepatic steatosis after 4 weeks of HFCD (**Figure 4A, B**). Although SH42 treatment largely increased plasma desmosterol levels also in LXR α -deficient mice (+80%, **Supplemental Figure 5E**), it failed to improve hepatic steatosis (**Figure 4A**) as evidenced by an unchanged steatosis score (**Figure 4B**) and similar lipid positive areas in SH42 treated mice compared to control (**Figure 4C**). Liver lipidomic analysis further revealed that almost no lipid species was significantly changed upon SH42 treatment as shown by volcano plot analysis (**Figure 4D**). Accordingly, SH42 treatment showed no effect on hepatic concentrations of TAG (**Figure 4E**), DAG (**Figure 4F**), FFA (**Figure 4G**) or CE (**Figure 4H**) in absence of LXR α .

The therapeutic effects of DHCR24 inhibition on Kupffer cell activation and hepatic monocyte infiltration are strictly dependent on LXR α

Subsequently, we analysed hepatic immune cells by flow cytometry after 4 weeks treatment with SH42 in HFCD-fed LXR α -deficient mice. In contrast to *E3L.CETP* mice, SH42 did not affect hepatic leukocytes (**Figure 5A**) in LXR α deficient mice. Strikingly, SH42 did not affect KC numbers (**Figure 5B, C**), and did not prevent KC activation as evidenced by unchanged high levels of NASH-associated MHCII⁺CD11c⁺ activated KCs (**Figure 5D, E**) and MHCII⁺CD11c⁻ resting KCs (**Figure 5D, F**). SH42 did not reduce recruited monocytes in liver (**Figure 5G**) but reduced hepatic neutrophils in LXR α -deficient mice (-42%; **Figure 5H**). Congruent with these data, circulating monocytes and neutrophils were not affected by SH42 treatment (**Supplemental Figure 6A-C**). Taken together, these data show that inhibition of DHCR24 by SH42 does not prevent diet-induced hepatic steatosis and inflammation in LXR α deficient mice.

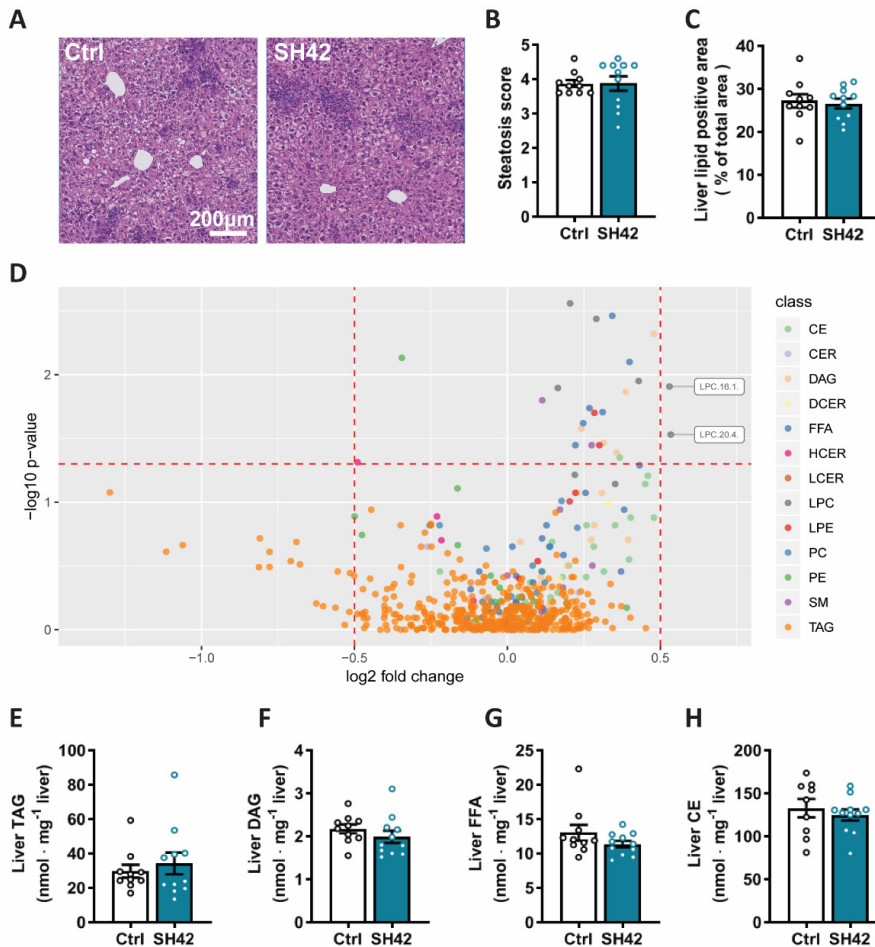


Figure 4. The therapeutic effects of DHCR24 inhibition on hepatic steatosis are strictly dependent on LXR α . LXR α deficient mice fed HFD were treated with vehicle or DHCR24 inhibitor SH42 (n= 10 and 11 mice, respectively). After 4 weeks of treatment, mice were sacrificed and liver samples were collected to stain with (A) HE. (B) Hepatic steatosis was scored and (C) lipid positive area was determined. (D) Volcano plot analysis of liver lipid species concentrations is shown. Annotated lipid species are characterized by a fold change >1.4 or <0.7 (SH42/Ctrl) and a p value <0.05. Hepatic (E) TAG, (F) DAG, (G) FFA and (H) CE lipid class concentrations were summarized. One outlier was identified and excluded in the hepatic CE analysis. Values are mean \pm SEM. Differences between two groups were determined using unpaired Student's t-test if not indicated otherwise. Abbreviations: CE, cholesteryl esters; CER, ceramides; DAG, diacylglycerols; DCER, dihydroceramides; FFA, free fatty acids; HCER, hexosylceramides; LPC, lysophosphatidylcholines; LPE, lysophosphatidylethanolamines; PC, phosphatidylcholines; PE, phosphatidylethanolamines; SM, sphingomyelins; TAG, triacylglycerols.

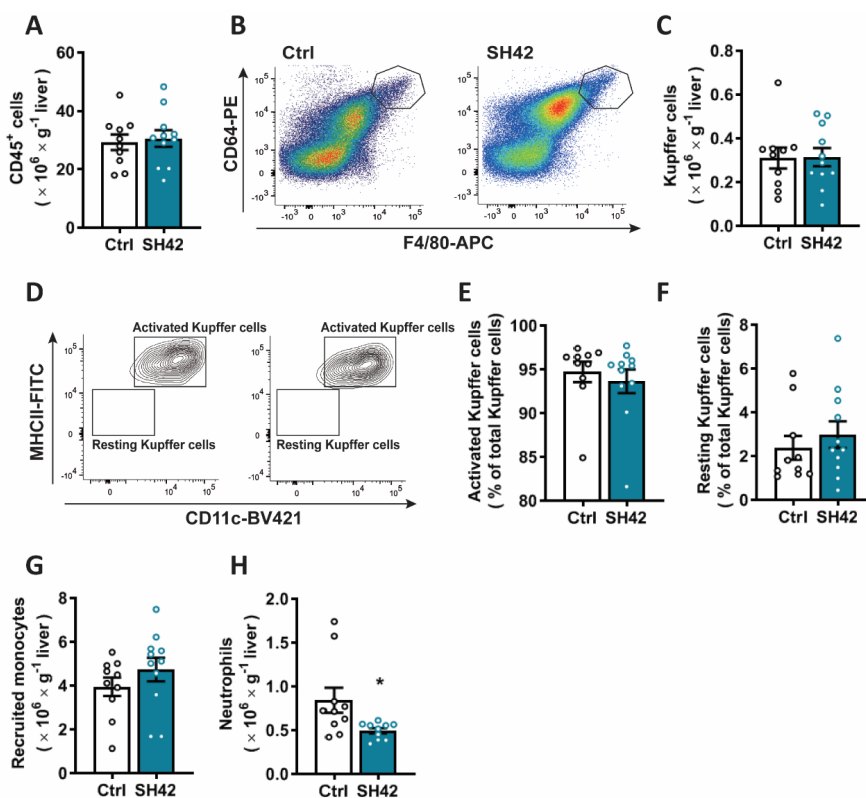


Figure 5. The therapeutic effects of DHCR24 inhibition on liver inflammation are strictly dependent on LXR α . LXR α deficient mice fed HFCD were treated with vehicle or DHCR24 inhibitor SH42 (n= 10 and 11 mice, respectively). After 4 weeks of treatment, mice were sacrificed and fresh liver samples were collected to isolate and count (A) CD45⁺ cells, (B and C) Total Kupffer cells (KCs), (D and E) activated KCs, (D and F) resting KCs, (G) recruited monocytes, and (H) neutrophils in the liver were measured via flow cytometry. Values are mean \pm SEM. Differences between two groups were determined using unpaired Student's t-test. *p<0.05 vs. ctrl.

Discussion

As key regulators of metabolic and inflammatory signaling [14, 15], LXRs have taken center stage as potential therapeutic targets for the treatment of cardiometabolic diseases. However, undesirable side effects of pharmacological LXR activation, including hyperlipidemia via induction of *Srebf1c* expression and neutropenia [24, 26], have prevented clinical application. Interestingly, desmosterol has been reported to be an endogenous ligand of LXR while inhibiting SREBP activity [29]. Therefore, enhancing endogenous desmosterol levels by targeting DHCR24 is already considered as a promising strategy for activating LXR transcription programs to combat atherosclerotic cardiovascular disease [28, 29, 39]. In this study, we exploited the synthetic DHCR24 inhibitor SH42, developed by our group [30], for the treatment of hepatic steatosis and inflammation, *i.e.*, the two hallmarks of NAFLD/NASH

development. We show that inhibition of DHCR24 induces marked increases in desmosterol levels in both liver and circulation which is accompanied by decreased hepatic steatosis and inflammation. Experiments performed in LXR α -deficient mice demonstrated that the therapeutic effects of SH42 are strictly dependent on LXR α activation, most likely due to increased desmosterol, as we have previously shown that SH42 does not have any intrinsic LXR affinity [23].

We found that inhibition of DHCR24 by SH42 markedly increased desmosterol levels in both *E3L.CETP* mice and LXR α -deficient mice, while SH42 prevented NASH-associated MHCII⁺CD11c⁺ KCs in *E3L.CETP* mice only (**Figure 2G-I**). This effect on KCs is likely attributed to the direct effects of desmosterol-induced LXR α activation in KCs. Indeed, it has been convincingly shown that desmosterol activates LXR in macrophages but not in hepatocytes [29, 40]. Consistently, we previously showed that inhibition of DHCR24 by SH42 increased desmosterol and induced the expression of LXR target genes, including *Abca1* and *Abcg1* in RAW 264.7 macrophages [23]. LXR α is highly expressed in KCs and the region of enhancers unique to KCs are enriched in LXR-regulating sequence motifs [41], indicating a role of LXRs in KC homeostasis. Accordingly, we here observed that about 95% of KCs in LXR α -deficient mice displayed markers indicative of activated KCs (*i.e.* MHCII⁺/CD11c⁺ KCs) versus less than 25% of KCs in wild type mice upon feeding the same HFCD, which is in agreement with our previous study in LXR α -deficient mice showing a robust increase in KC activation and hepatic inflammation [37]. Taken together, our study suggests that pharmacological inhibition of DHCR24 is a feasible way to prevent KC activation and alleviate liver inflammation through desmosterol-induced LXR α activation.

Importantly, we observed that inhibition of DHCR24 by SH42 reduced liver lipids including TAG and DAG and hence alleviated hepatic steatosis in *E3L.CETP* mice (**Figure 1**) but not in LXR α -deficient mice (**Figure 4**). We excluded the potential contribution of altered systemic glucose homeostasis in this process as evidenced by unchanged body composition, circulating glucose and insulin levels, as well as HOMA-IR scores in both groups (**Supplemental Figure 1**). We reasoned that the alleviated liver inflammation may largely contribute to the reduction of hepatic steatosis. The feed-forward loop between lipotoxic hepatocytes and proinflammatory immune cells, especially KCs, promotes NAFLD/NASH progression [42]. Our study strongly suggests that this vicious circle can be abrogated by desmosterol-induced LXR α activation in liver-resident KCs. Consistently, both prevention of KC activation and depletion of KCs reduces liver inflammation [43] and alleviates hepatic steatosis [9, 10]. Therefore, the alleviated liver inflammation could be the direct effect of desmosterol in macrophages/KCs, which subsequently reduces hepatic steatosis and prevents NAFLD/NASH progression.

Pharmaceutical development of LXR agonists has been challenged by the fact that these compounds usually induce *de novo* lipogenesis [24, 26], which is mainly attributable to hepatocyte-specific LXR α activation [44, 45]. Therefore, it is of great interest that DHCR24 inhibition by SH42 decreases plasma FFA and CE levels, without increasing plasma total TAG and DAG levels (**Figure 3**), which implies that LXR α activation by desmosterol, in contrast to synthetic agonists, does not lead to hyperlipidemia. This can be easily understood from the fact that desmosterol activates LXR α in macrophages/KCs only, whereas LXR-induced hyperlipidemia is mainly due to increased *de novo* lipogenesis within hepatocytes [29]. In fact, desmosterol was even reported to suppress SREBPs in macrophages via an Insig/SREBP cleavage-activating protein (SCAP)-dependent mechanism [28, 29, 39]. Taken together, SH42-induced desmosterol does not evoke an undesirable increase in plasma and hepatic lipid levels that are typical for synthetic LXR agonists, likely by selective LXR α activation in

macrophages/KC rather than hepatocytes.

A human study has demonstrated that desmosterol levels in circulation and liver are associated with NASH development [46]. However, whether desmosterol has a specific role in the pathophysiology of NAFLD/NASH is still unknown. To the best of our knowledge, our present study for the first time shows the potential application of pharmacological DHCR24 inhibition to enhance endogenous desmosterol levels for the treatment of NAFLD/NASH. Interestingly, a recent genetic study demonstrated that the rs588709 variant near the *DHCR24* locus is associated with lower circulating TAG-rich VLDL particles [47], which potentially extends the role of DHCR24 to human lipid metabolism. Triparanol is the most widely used (nonspecific) DHCR24 inhibitor [48]; however, it was withdrawn from clinical application due to severe adverse side effects, such as nausea and vomiting, cataracts, and skin disorders [49]. In contrast to Triparanol with an IC_{50} value of 14 μ M, SH42 is a much more selective and potent DHCR24 inhibitor having an IC_{50} value of less than 10 nM in a cellular assay [30, 50]. In our preclinical mouse model, we did not observe adverse effects of SH42 treatment on food intake, body weight, and body composition. Additionally, desmosterol-induced LXR activation via inhibition of DHCR24 did not cause a reduction of circulating neutrophils or neutropenia, another adverse effect of systemic LXR activation [26]. These advantages of targeting DHCR24 over synthetic LXR agonists will possibly lead to a promising application of DHCR24 inhibitors to combat NAFLD/NASH, in addition to other cardiometabolic and inflammatory diseases.

In conclusion, we show that pharmacological inhibition of DHCR24 increases desmosterol to prevent diet-induced hepatic steatosis and inflammation, two main hallmarks of NAFLD/NASH development, without inducing hyperlipidemia. As such, our study paves the way for developing a new therapeutic strategy for the treatment for NAFLD/NASH.

Acknowledgements

This work was supported by the Netherlands Organisation for Scientific Research-NWO (VENI grant 91617027 to Y.W.); the Netherlands Organisation for Health Research and Development-ZonMW (Early Career Scientist Hotel grant 435004007 to Y.W.); the Netherlands Cardiovascular Research Initiative: an initiative with support of the Dutch Heart Foundation (CVON-GENIUS-2 to P.C.N.R., CVON-IN CONTROL-2 to F.K.); and the Netherlands Heart Foundation (2009T038 to P.C.N.R.). M.G. was partially supported by the Netherlands X-omics initiative which is partially funded by NWO, project 184.034.019. Y.W. is supported by the China “Thousand Talents Plan” (Young Talents), Shaanxi province “Thousand Talents Plan” (Young Talents) and Foundation of Xi’an Jiaotong University (Plan A). E.Z. is supported by the China Scholarship Council (CSC, grant 201606010321).

Author contributions

E.Z. designed the study, performed experiments, analysed the data, and drafted the manuscript. H.N., R.L., H.J.P.Z., C.L., Z.L. and J.F.B. contributed to animal experiments and analysed the data. C.M. and F.B. provided SH42 compound. Y.M., F.K. and B.G. interpreted data and revised manuscript. P.C.N.R. and M.G. obtained financial support, designed the study and revised the manuscript. Y.W. obtained financial support, designed the study, analysed the data, and drafted the manuscript.

Conflict of interest

The authors have no conflicts of interest to disclose.

References

1. Berlanga, A., et al., *Molecular pathways in non-alcoholic fatty liver disease*. Clin Exp Gastroenterol, 2014. **7**: p. 221-39.
2. Chalasani, N., et al., *The diagnosis and management of nonalcoholic fatty liver disease: Practice guidance from the American Association for the Study of Liver Diseases*. Hepatology, 2018. **67**(1): p. 328-357.
3. Younossi, Z.M., et al., *Global epidemiology of nonalcoholic fatty liver disease-Meta-analytic assessment of prevalence, incidence, and outcomes*. Hepatology, 2016. **64**(1): p. 73-84.
4. Baffy, G., *Kupffer cells in non-alcoholic fatty liver disease: the emerging view*. J Hepatol, 2009. **51**(1): p. 212-23.
5. Wandrer, F., et al., *TNF-Receptor-1 inhibition reduces liver steatosis, hepatocellular injury and fibrosis in NAFLD mice*. Cell Death Dis, 2020. **11**(3): p. 212.
6. Aparicio-Vergara, M., et al., *Tumor necrosis factor receptor 1 gain-of-function mutation aggravates nonalcoholic fatty liver disease but does not cause insulin resistance in a murine model*. Hepatology, 2013. **57**(2): p. 566-76.
7. Schuster, S., et al., *Triggering and resolution of inflammation in NASH*. Nat Rev Gastroenterol Hepatol, 2018. **15**(6): p. 349-364.
8. Tosello-Tramont, A.C., et al., *Kupffer cells trigger nonalcoholic steatohepatitis development in diet-induced mouse model through tumor necrosis factor-alpha production*. J Biol Chem, 2012. **287**(48): p. 40161-72.
9. Huang, W., et al., *Depletion of liver Kupffer cells prevents the development of diet-induced hepatic steatosis and insulin resistance*. Diabetes, 2010. **59**(2): p. 347-57.
10. Lanthier, N., et al., *Kupffer cell depletion prevents but has no therapeutic effect on metabolic and inflammatory changes induced by a high-fat diet*. FASEB J, 2011. **25**(12): p. 4301-11.
11. Bieghs, V., et al., *Trapping of oxidized LDL in lysosomes of Kupffer cells is a trigger for hepatic inflammation*. Liver Int, 2013. **33**(7): p. 1056-61.
12. Tran, S., et al., *Impaired Kupffer Cell Self-Renewal Alters the Liver Response to Lipid Overload during Non-alcoholic Steatohepatitis*. Immunity, 2020. **53**(3): p. 627-640 e5.
13. Remmerie, A., et al., *Osteopontin Expression Identifies a Subset of Recruited Macrophages Distinct from Kupffer Cells in the Fatty Liver*. Immunity, 2020. **53**(3): p. 641-657 e14.
14. Ito, A., et al., *LXRs link metabolism to inflammation through Abca1-dependent regulation of membrane composition and TLR signaling*. Elife, 2015. **4**: p. e08009.
15. Bensinger, S.J. and P. Tontonoz, *Integration of metabolism and inflammation by lipid-activated nuclear receptors*. Nature, 2008. **454**(7203): p. 470-7.
16. Prufer, K. and J. Boudreaux, *Nuclear localization of liver X receptor alpha and beta is differentially regulated*. J Cell Biochem, 2007. **100**(1): p. 69-85.
17. Venkateswaran, A., et al., *Control of cellular cholesterol efflux by the nuclear oxysterol receptor LXR alpha*. Proc Natl Acad Sci U S A, 2000. **97**(22): p. 12097-102.
18. Bischoff, E.D., et al., *Non-redundant roles for LXRalpha and LXRbeta in atherosclerosis susceptibility in low density lipoprotein receptor knockout mice*. J Lipid Res, 2010. **51**(5): p. 900-6.
19. Ishibashi, M., et al., *Knock-down of the oxysterol receptor LXRalpha impairs cholesterol efflux in human primary macrophages: lack of compensation by LXRbeta activation*. Biochem Pharmacol, 2013. **86**(1): p. 122-9.
20. Joseph, S.B., et al., *LXR-dependent gene expression is important for macrophage*

21. Wang, Y.Y., et al., *Activation of the liver X receptor protects against hepatic injury in endotoxemia by suppressing Kupffer cell activation*. Shock, 2006. **25**(2): p. 141-6.
22. Li, P., et al., *NCoR repression of LXRs restricts macrophage biosynthesis of insulin-sensitizing omega 3 fatty acids*. Cell, 2013. **155**(1): p. 200-214.
23. Korner, A., et al., *Inhibition of Delta24-dehydrocholesterol reductase activates pro-resolving lipid mediator biosynthesis and inflammation resolution*. Proc Natl Acad Sci U S A, 2019. **116**(41): p. 20623-20634.
24. Grefhorst, A., et al., *Stimulation of lipogenesis by pharmacological activation of the liver X receptor leads to production of large, triglyceride-rich very low density lipoprotein particles*. J Biol Chem, 2002. **277**(37): p. 34182-90.
25. Schultz, J.R., et al., *Role of LXRs in control of lipogenesis*. Genes Dev, 2000. **14**(22): p. 2831-8.
26. Kirchgessner, T.G., et al., *Beneficial and Adverse Effects of an LXR Agonist on Human Lipid and Lipoprotein Metabolism and Circulating Neutrophils*. Cell Metab, 2016. **24**(2): p. 223-33.
27. Nes, W.D., *Biosynthesis of cholesterol and other sterols*. Chem Rev, 2011. **111**(10): p. 6423-51.
28. Spann, N.J., et al., *Regulated accumulation of desmosterol integrates macrophage lipid metabolism and inflammatory responses*. Cell, 2012. **151**(1): p. 138-52.
29. Muse, E.D., et al., *Cell-specific discrimination of desmosterol and desmosterol mimetics confers selective regulation of LXR and SREBP in macrophages*. Proc Natl Acad Sci U S A, 2018. **115**(20): p. E4680-E4689.
30. Muller, C., et al., *New chemotype of selective and potent inhibitors of human delta 24-dehydrocholesterol reductase*. Eur J Med Chem, 2017. **140**: p. 305-320.
31. Westerterp, M., et al., *Cholesteryl ester transfer protein decreases high-density lipoprotein and severely aggravates atherosclerosis in APOE*3-Leiden mice*. Arterioscler Thromb Vasc Biol, 2006. **26**(11): p. 2552-9.
32. Plosch, T., et al., *Abcg5/Abcg8-independent pathways contribute to hepatobiliary cholesterol secretion in mice*. Am J Physiol Gastrointest Liver Physiol, 2006. **291**(3): p. G414-23.
33. Alarcon-Barrera, J.C., et al., *Lipid metabolism of leukocytes in the unstimulated and activated states*. Anal Bioanal Chem, 2020. **412**(10): p. 2353-2363.
34. Liang, W., et al., *Establishment of a general NAFLD scoring system for rodent models and comparison to human liver pathology*. PLoS One, 2014. **9**(12): p. e115922.
35. Itoh, M., et al., *Hepatic crown-like structure: a unique histological feature in non-alcoholic steatohepatitis in mice and humans*. PLoS One, 2013. **8**(12): p. e82163.
36. Peet, D.J., et al., *Cholesterol and bile acid metabolism are impaired in mice lacking the nuclear oxysterol receptor LXR alpha*. Cell, 1998. **93**(5): p. 693-704.
37. Endo-Umeda, K., et al., *Dysregulation of Kupffer Cells/Macrophages and Natural Killer T Cells in Steatohepatitis in LXRalpha Knockout Male Mice*. Endocrinology, 2018. **159**(3): p. 1419-1432.
38. Endo-Umeda, K. and M. Makishima, *Liver X Receptors Regulate Cholesterol Metabolism and Immunity in Hepatic Nonparenchymal Cells*. Int J Mol Sci, 2019. **20**(20).
39. Rodriguez-Acebes, S., et al., *Desmosterol can replace cholesterol in sustaining cell proliferation and regulating the SREBP pathway in a sterol-Delta24-reductase-deficient cell line*. Biochem J, 2009. **420**(2): p. 305-15.
40. Snodgrass, R.G., et al., *Efferocytosis potentiates the expression of arachidonate*

- 15-lipoxygenase (ALOX15) in alternatively activated human macrophages through LXR activation.* Cell Death Differ, 2020.
41. Lavin, Y., et al., *Tissue-resident macrophage enhancer landscapes are shaped by the local microenvironment.* Cell, 2014. **159**(6): p. 1312-26.
 42. Hirsova, P. and G.J. Gores, *Death Receptor-Mediated Cell Death and Proinflammatory Signaling in Nonalcoholic Steatohepatitis.* Cell Mol Gastroenterol Hepatol, 2015. **1**(1): p. 17-27.
 43. Bieggs, V., et al., *Specific immunization strategies against oxidized low-density lipoprotein: a novel way to reduce nonalcoholic steatohepatitis in mice.* Hepatology, 2012. **56**(3): p. 894-903.
 44. Bradley, M.N., et al., *Ligand activation of LXR beta reverses atherosclerosis and cellular cholesterol overload in mice lacking LXR alpha and apoE.* J Clin Invest, 2007. **117**(8): p. 2337-46.
 45. Zhang, Y., et al., *Liver LXRalpha expression is crucial for whole body cholesterol homeostasis and reverse cholesterol transport in mice.* J Clin Invest, 2012. **122**(5): p. 1688-99.
 46. Simonen, M., et al., *Desmosterol in human nonalcoholic steatohepatitis.* Hepatology, 2013. **58**(3): p. 976-82.
 47. Sliz, E., et al., *A variant near DHCR24 associates with microstructural properties of white matter and peripheral lipid metabolism in adolescents.* Mol Psychiatry, 2020.
 48. Muller, C., et al., *A gas chromatography-mass spectrometry-based whole-cell screening assay for target identification in distal cholesterol biosynthesis.* Nat Protoc, 2019. **14**(8): p. 2546-2570.
 49. Kirby, T.J., *Cataracts produced by triparanol. (MER-29).* Trans Am Ophthalmol Soc, 1967. **65**: p. 494-543.
 50. Moebius, F.F., et al., *Molecular cloning and expression of the human delta7-sterol reductase.* Proc Natl Acad Sci U S A, 1998. **95**(4): p. 1899-902.

Supplemental appendix

Supplemental materials and methods

Plasma glucose and insulin assay

Four hour-fasted (9 am till 1 pm) blood samples were collected via tail vein of *E3L.CETP* mice bleeding into heparin-coated capillaries after 8 weeks treatment with vehicle or SH42. Blood samples were then centrifuged and plasma was assayed for glucose (INStruchemie, The Netherlands) and insulin (Mercodia AB, Sweden) according to the manufacturers' protocols. The homeostatic Model Assessment for Insulin Resistance (HOMA-IR) scores were calculated using the equation: $\text{HOMA-IR} = \text{fasting insulin (mU}\cdot\text{L}^{-1}) \times \text{fasting glucose (mmol}\cdot\text{L}^{-1}) / 22.5$ [1].

Liver histology and hepatic steatosis scoring

After 8 weeks of treatment in *E3L.CETP* mice or 4 weeks in LXR α -deficient mice, mice were sacrificed and transcardially perfused with cold PBS, and livers were collected and fixed in phosphate-buffered 4% formaldehyde. Fixed tissues were embedded in paraffin and cut into sections of 5 μm thickness for staining with hematoxylin and eosin (HE) and/or the macrophage marker F4/80 (1 $\mu\text{g}\cdot\text{mL}^{-1}$, MCA497, Serotec, Oxford, UK) which was detected using ImmPRESS HRP goat anti-rat IgG detection kit (MP-744-15, Vector Laboratories, CA, USA). Hepatic steatosis was evaluated from HE stained slides by two blinded experts respectively, with the criteria proposed by Liang *et al* [2] with slight modification. Hepatocellular vesicular steatosis, *i.e.* microvesicular steatosis and macrovesicular steatosis, and hepatocellular hypertrophy were scored (grade 0 - 3) based on the percentage of the total area affected, and the grades were summed into one standard as "steatosis score" (0 - 9). Liver lipid positive area and F4/80 positive area were quantified using ImageJ software (version 1.50i). Hepatic crown-like structures formed by macrophages aggregating around dead hepatocytes were counted from F4/80 stained slides which were blinded before analysis and expressed as number per area [3]. Values in figures for each staining present means of 9 randomly selected image fields (0.468 mm^2 per field) per mouse. The antibody used is listed in **Supplemental Table 1**.

GC-MS analysis of desmosterol

After 8 weeks of treatment in *E3L.CETP* mice or 4 weeks in LXR α -deficient mice, desmosterol levels were measured using GC-MS after alkaline hydrolysis, as described previously for plasma [4] and liver [5]. In brief, a Bruker Scion GC-MS system or an Agilent 7890B coupled to a 5977B MS were utilized and operated in selected ion monitoring mode (SIM). An Agilent VF-5ms column, 25 m \times 0.25 mm \times 0.25 μm was used. Helium 99.9990% was used as carrier gas at a constant flow rate of 1.4 mL per min. Injector and transfer line were operated at 280°C. The oven program started at 90°C held for 0.5 min, then ramped to 270°C at 30°C per min, and ramped to 310°C at 10°C per min. The following masses were used to quantify desmosterol levels against an external calibration line (0 - 10 ppm) m/z 445 + 355 for cholestanol (IS), m/z 357 and 271 for cholestan (IS) and m/z 343 + 253 or 441.2 for desmosterol. Desmosterol was identified by matching characteristic ions and retention times with an authentic standard (Sigma Aldrich).

Quantitative lipidomic analysis

Quantitative lipidomic analysis was carried out in liver and plasma samples in *E3L.CETP* mice and in LXR α -deficient mice as described elsewhere [5]. Briefly, a small piece of liver tissue was homogenized with 600 μL LCMS grade water in a bullet blender for 30 sec and an aliquot corresponding to 5 mg liver tissue was used. For plasma samples, 25 μL was used.

25 μ L internal standard mix (100 μ L for liver samples) (Lipidyzer™ internal standard kit, containing >50 labelled internal standards for 13 lipid classes, Sciex cat# 504156), 500 μ L methyl tert-butyl ether (MTBE), and 160 μ L methanol were subsequently added and the mixture was shaken for 30 min at room temperature. After adding 200 μ L water, samples were centrifuged at 16,000 g for 3 min and the upper organic layer was collected in a glass vial. The remaining sample was extracted again by adding 300 μ L MTBE, 100 μ L methanol and 100 μ L water for 30 min. The organic extracts were then pooled and dried under a gentle stream of nitrogen. The dry extract was subsequently dissolved in 250 μ L Lipidyzer running buffer and analysed according to the manufacturer's protocol. For data analysis, 13 lipid classes, including cholesteryl esters (CE), ceramides (CER), diacylglycerols (DAG), dihydroceramides (DCER), free fatty acids (FFA), hexosylceramides (HCER), lysophosphatidylcholines (LPC), lysophosphatidylethanolamines (LPE), phosphatidylcholines (PC), phosphatidylethanolamines (PE), sphingomyelins (SM) and triacylglycerols (TAG) were compared.

Isolation of liver immune cells and peripheral blood mononuclear cells

After 4 weeks of SH42 treatment, blood and liver was collected and processed for flow cytometry as described previously [6]. In short, blood was collected from the retro-orbital sinus of anesthetized mice into heparin capillaries, after which mice were sacrificed and transcardially perfused with PBS for 5 min to remove circulating cells. Livers were collected and minced with a scalpel to form a paste, digested with collagenase type IV (Sigma Aldrich, US), and hepatocytes were removed by low gravity centrifugation at 50 g for 3 min. CD45⁺ leukocytes were isolated using CD45 microbeads (35 μ L beads per liver; Miltenyi Biotec, US) and an LS column, according to the manufacturer's instructions. In addition, peripheral blood mononuclear cells were isolated. To this end, 450 μ L blood was mixed with red blood cell lysis/fix buffer (Becton Dickinson, US) (3:20; v/v) for 15 min at room temperature. Subsequently, white blood cells were pelleted by centrifugation at 600 g for 5 min. The supernatant was discarded and cells were resuspended and washed with PBS. The cells isolated from the liver and blood were counted and characterized by flow cytometry.

6

Flow cytometry analysis

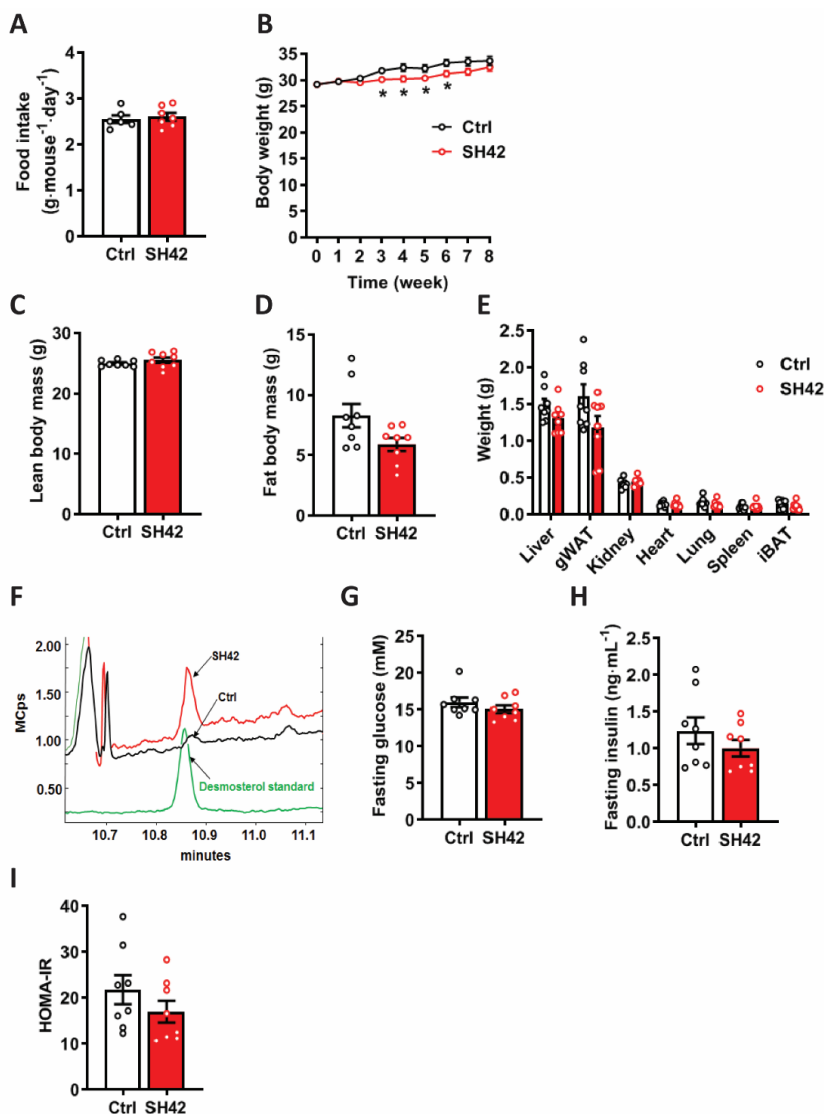
All cell suspensions were stained with the fixable viability dye Zombie-UV (BioLegend, US) and fixed with 1.9% paraformaldehyde. Within 24 h of fixation, the cells were pre-incubated with an Fc γ blocking antibody (Thermo Fisher Scientific) for 15 min. The cells were then stained with fluorescently labelled antibodies listed in **Supplemental Table 2** for 30 min at 4°C in the dark. Fluorescently labelled cells were measured on an LSRII (Becton Dickinson) and gates were set according to Fluorescence Minus One (FMO) controls using FlowJo™ Software (Becton Dickinson). Representative gating schemes are shown in **Supplemental Figure 7 and 8**.

Supplemental Table 1. Antibodies used for immunohistochemistry

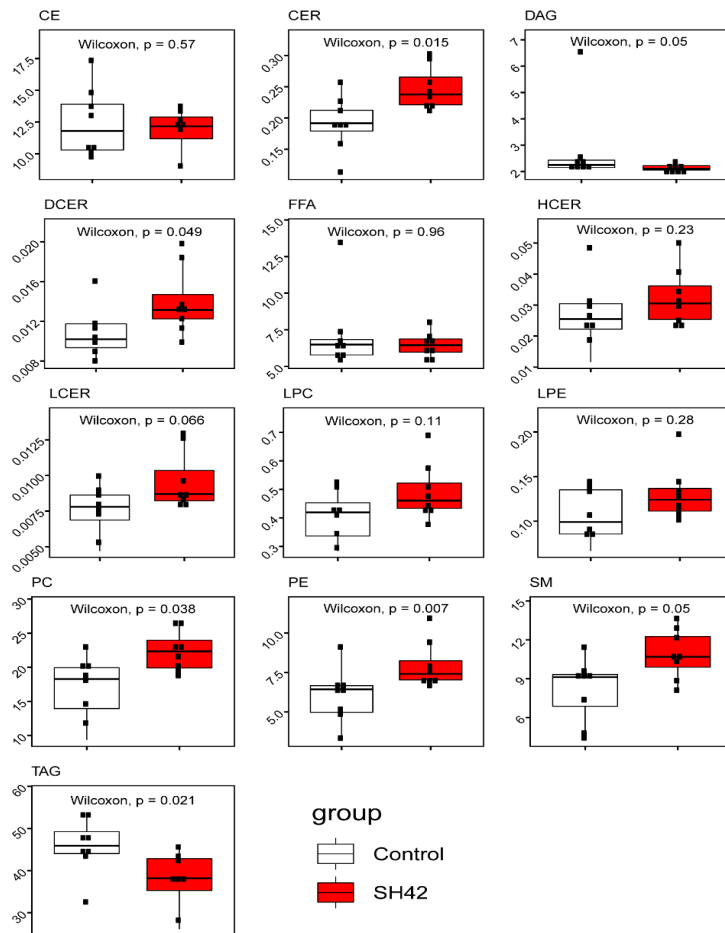
Target	Concentration used	Vendor	Catalog No.
F4/80	1 $\mu\text{g}\cdot\text{mL}^{-1}$	Serotec, Oxford, UK	MCA497

Supplemental Table 2. Antibodies used for flow cytometry

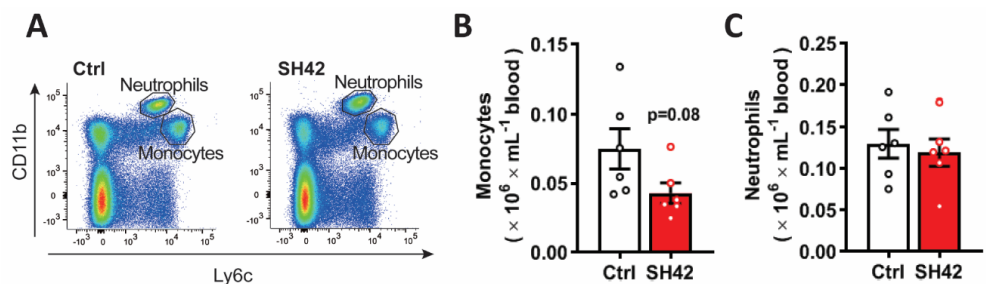
Fluorophore	Target	Clone	Vendor
FITC	MHCII	M5/114.15.2	Biolegend
PE	CD64	X54-5/7.1	Biolegend
PE-Cy7	CD11b	M1/70	eBioscience
APC	F4/80	BM8	eBioscience
APC-Cy7	Ly6C	HK1.4	Biolegend
BV421	CD11c	N418	Biolegend
BV605	Siglec-F	E50-2440	BD Biosciences
BV785	CD45	30F11	Biolegend



Supplemental Figure 1. Inhibition of DHCR24 by SH42 does not affect food intake, body composition, organ weight, and plasma glucose and insulin levels, while increasing plasma desmosterol levels. *E3L.CETP* mice fed a high fat high cholesterol diet (HFCD) were treated with vehicle or DHCR24 inhibitor SH42 (n= 8 mice per group). (A) Food intake was measured during week 3 to 6 (n= 6 and 7 cages, respectively). (B) Body weight was measured weekly and (C) lean body mass and (D) fat body mass were determined at the end of week 8. After 8 weeks of treatment, mice were sacrificed and (E) organs were collected and weighted. Four hour-fasted blood samples were collected before the sacrifice to measure (F) desmosterol levels and (G) glucose and (H) insulin levels. (I) The homeostatic Model Assessment for Insulin Resistance (HOMA-IR) scores were calculated. Values are mean \pm SEM. Differences between two groups were determined using unpaired Student's t-test. *P<0.05 vs. ctrl. Abbreviations: gWAT, gonadal white adipose tissue; iBAT, interscapular brown adipose tissue.

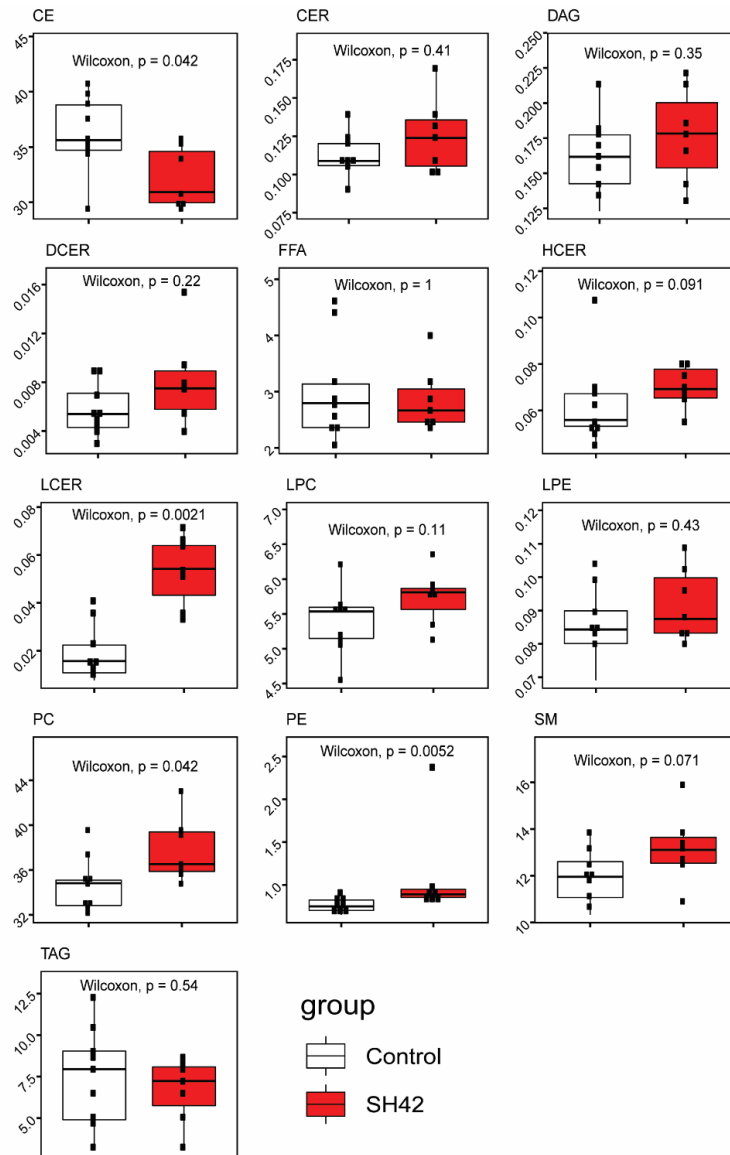


Supplemental Figure 2. Inhibition of DHCR24 by SH42 alters liver lipid class compositions. *E3L.CETP* mice fed a HFCD were treated with vehicle or DHCR24 inhibitor SH42 (n= 8 mice per group). After 8 weeks of treatment, mice were sacrificed and livers were collected to determine liver lipid class compositions. The boxplot indicates 1st quartile, median, and 3rd quartile. Differences between two groups were determined using Wilcoxon rank sum test. Abbreviations: CE, cholesteryl esters; CER, ceramides; DAG, diacylglycerols; DCER, dihydroceramides; FFA, free fatty acids; HCER, hexosylceramides; LPC, lysophosphatidylcholines; LPE, lysophosphatidylethanolamines; PC, phosphatidylcholines; PE, phosphatidylethanolamines; SM, sphingomyelins; TAG, triacylglycerols.

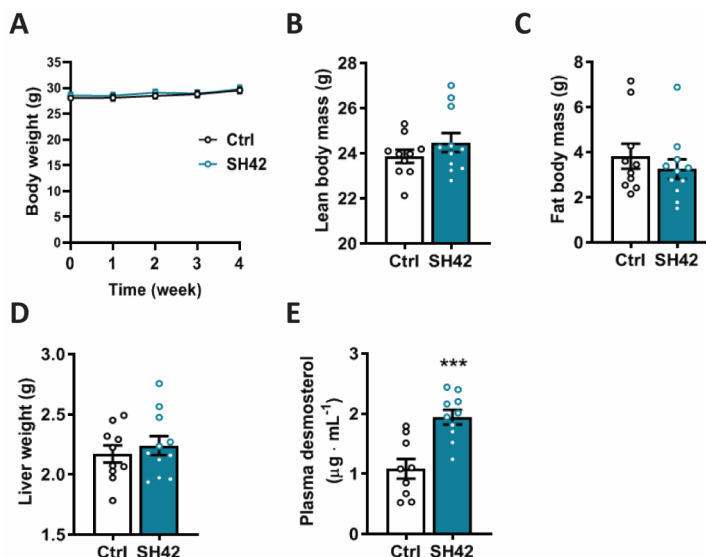


6

Supplemental Figure 3. Inhibition of DHCR24 by SH42 tends to reduce circulating monocytes while no effect on circulating neutrophils. *E3L.CETP* mice fed a HFCD were treated with vehicle or DHCR24 inhibitor SH42 (n= 6 mice per group). After 4 weeks of treatment, blood samples were collected to measure (A and B) monocytes and (A and C) neutrophils via flow cytometry. Values are mean ± SEM. Differences between two groups were determined using unpaired Student's t-test.

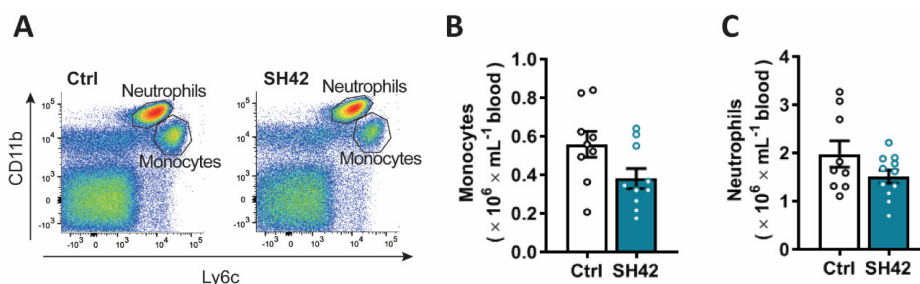


Supplemental Figure 4. Inhibition of DHCR24 by SH42 does not increase plasma DAG and TAG fractions. *E3L.CETP* mice fed a HFD were treated with vehicle or DHCR24 inhibitor SH42 (n= 8 mice per group). After 8 weeks of treatment, blood samples were collected to determine lipid class compositions. The boxplot indicates 1st quartile, median, and 3rd quartile. Differences between two groups were determined using Wilcoxon rank sum test. Abbreviations: CE, cholesteryl ester; CER, ceramides; DAG, diacylglycerols; DCER, dihydroceramides; FFA, free fatty acids; HCER, hexosylceramides; LPC, lysophosphatidylcholines; LPE, lysophosphatidylethanolamines; PC, phosphatidylcholines; PE, phosphatidylethanolamines; SM, sphingomyelins; TAG, triacylglycerols.

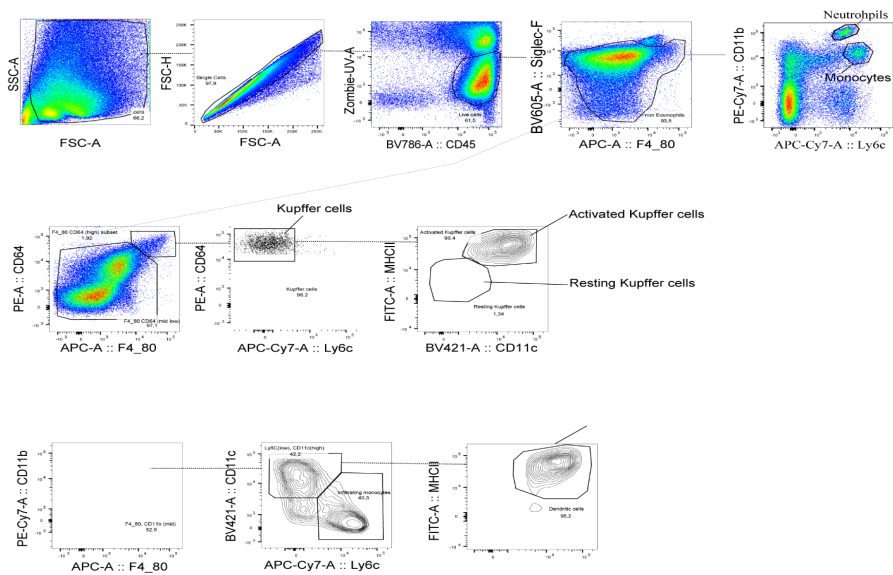


Supplemental Figure 5. Inhibition of DHCR24 by SH42 does not affect body weight, body composition or liver weight, while increasing plasma desmosterol levels in LXR α -deficient mice. LXR α deficient mice fed HFCD were treated with vehicle or DHCR24 inhibitor SH42 (n= 10 and 11 mice, respectively). (A) Body weight was measured weekly. After 4 weeks of treatment, (B) lean body mass and (C) fat body mass were determined. Mice were sacrificed and (D) livers were collected and weighted. (E) Plasma desmosterol levels were measured at the end of the experiment (n= 9 and 11 mice respectively; one sample in control group was lost due to technical failure). Values are mean \pm SEM. Differences between two groups were determined using unpaired Student's t-test. ***P<0.001 vs. ctrl.

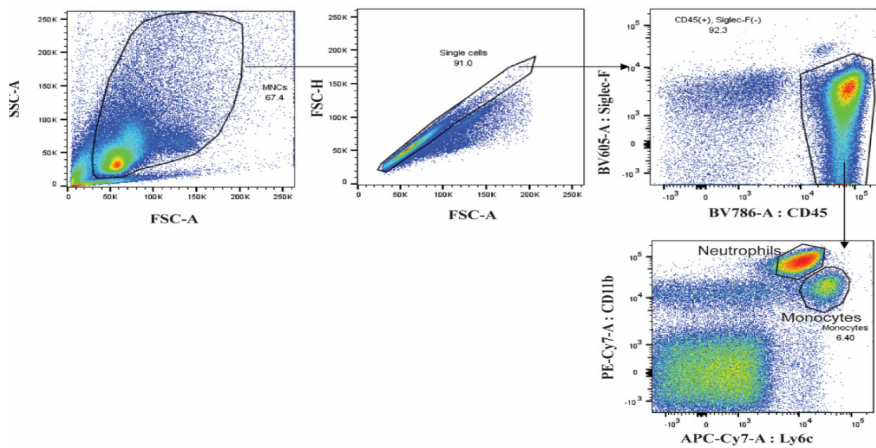
6



Supplemental Figure 6. Inhibition of DHCR24 by SH42 does affect circulating monocytes and neutrophils in LXR α -deficient mice. LXR α deficient mice fed HFCD were treated with vehicle or DHCR24 inhibitor SH42 (n= 10 and 11 mice respectively). After 4 weeks of treatment, blood samples were collected to measure (A and B) monocytes (n= 9 and 10 mice respectively; two values were identified as outliers based on Grubbs' test and removed from statistical analysis) and (A and C) neutrophils were determined (n= 9 and 11 mice respectively; one value was identified as an outlier based on Grubbs' test and removed from statistical analysis) via flow cytometry analysis. Values are mean \pm SEM. Differences between two groups were determined using unpaired Student's t-test.



Supplemental Figure 7. Representative gating scheme for FACS analysis in liver samples.



Supplemental Figure 8. Representative gating scheme for FACS analysis in blood samples

Supplemental references

1. Matthews, D.R., et al., *Homeostasis model assessment: insulin resistance and beta-cell function from fasting plasma glucose and insulin concentrations in man*. Diabetologia, 1985. **28**(7): p. 412-9.
2. Liang, W., et al., *Establishment of a general NAFLD scoring system for rodent models and comparison to human liver pathology*. PLoS One, 2014. **9**(12): p. e115922.
3. Itoh, M., et al., *Hepatic crown-like structure: a unique histological feature in non-alcoholic steatohepatitis in mice and humans*. PLoS One, 2013. **8**(12): p. e82163.
4. Muller, C., et al., *New chemotype of selective and potent inhibitors of human delta 24-dehydrocholesterol reductase*. Eur J Med Chem, 2017. **140**: p. 305-320.
5. Korner, A., et al., *Inhibition of Delta24-dehydrocholesterol reductase activates pro-resolving lipid mediator biosynthesis and inflammation resolution*. Proc Natl Acad Sci U S A, 2019. **116**(41): p. 20623-20634.
6. Husaarts, L., et al., *Chronic helminth infection and helminth-derived egg antigens promote adipose tissue M2 macrophages and improve insulin sensitivity in obese mice*. FASEB J, 2015. **29**(7): p. 3027-39.